Original Research

Safety of Metallic Implants in Magnetic Resonance Imaging

Henry S. Ho*

Magnetic resonance (MR) imaging has become a commonly accepted medical procedure. Manufacturers of medical implant devices are submitting claims that their devices are safe and effective in a MR environment. This paper concentrates on the issue of heating of patients due to the interaction of metallic implants with the strong radiofrequency (RF) magnetic field produced by the MR scanner. The commercially available program XFDTD was used to calculate the specific absorption rate (SAR) distribution in a realistic model of the human body. The body contained a metallic implant and was exposed to RF magnetic fields at 64 MHz from a model of a MR birdcage body coil. The results of the calculation showed that the magnitude of the increased heating of tissues due to the presence of the metallic implant depended on the dimensions, orientation, shape, and location of the metallic implant in the patient. This increased heating of surrounding tissues primarily concentrates in a small volume near the tip of the metallic wire. When the whole-body SAR was normalized to 1 W/kg, a calculated value of 41 W/kg was obtained at this location if the absorption was averaged over 1 g of tissue. However, a maximum value of 310 W/kg was calculated when the absorption was averaged over 1/8 g of tissue. J. Magn. Reson. Imaging 2001; 14:472–477. Published 2001 Wiley-Liss, Inc.†

Index terms: MRI; safety; heating; leads; implants; SAR

MAGNETIC RESONANCE (MR) IMAGING has become a commonly accepted medical procedure with wide usage (1). Conventional MR imaging systems with static magnetic fields at or below 3 Tesla, and open MR imaging systems up to 0.7 Tesla, are in widespread use. Higher static magnetic field MR devices ranging from 3 Tesla to 8 Tesla are being used in investigational studies.

A MR device produces a pulsed radiofrequency (RF) magnetic field with a frequency proportional to the value of the static magnetic field strength of the device. For example, a 1.5-Tesla MR device produces a RF magnetic field of 64 MHz. The RF magnetic field interacts with the patient's tissues, resulting in the absorption of RF energy by the tissues. The specific absorption rate (SAR), with units of W/kg, denotes the rate of energy absorption. Reported SAR values are often averaged over a specified volume of tissue. The RF energy absorbed by the patient, averaged over the whole body, is called whole body averaged SAR. The SAR values at individual points usually occur in non-uniform patterns within the patient's body. A metallic implant in the patient's body interacts with the RF magnetic field of the MR scanner, resulting in a concentration of local RF heating in the patient's tissues near the implant.

Newer, open MR imaging systems have increasingly been used in various medical practices, including interventional procedures. This has created the need for medical instruments and devices that can be used very close to the patient during MR imaging, in an environment with high static and RF magnetic fields. Increasingly, manufacturers are claiming that their devices, including metallic implants in the patient's body, are safe and effective in a MR environment (2–4). Some have made changes to their devices in making these claims.

This study used computer modeling of electromagnetic field theory to calculate the enhanced RF heating of tissues surrounding metallic implants of patients during MR imaging. This calculation did not include the determination of temperature rises in tissues due to RF heating. While high SAR values may indicate the potential for temperature rises in the tissues, the resultant temperature rises in tissues depend on the thermal properties of tissues, the thermal diffusion mechanisms of the body, and perhaps the RF pulse duration and duty cycles.

METHODS

XFDTD Method

The commercially available program XFDTD (5) was used to calculate the SAR distribution in a realistic model of the human body. The body contained a metallic implant and was exposed to a RF magnetic field at 64 MHz from a model of a MR birdcage body coil.

The XFDTD program used the finite difference time domain (FDTD) method (6) to calculate the electromagnetic field distributions in three dimensions in the model of the human body by solving the electromag-

Center for Devices and Radiological Health, Food and Drug Administration, Rockville, Maryland.

The mention of commercial products, their source, or their use in connection with material reported herein is not to be construed as either an actual or an implied endorsement of such products by the U.S. Food and Drug Administration.

*Address reprint requests to H.S.H., Center for Devices and Radiological Health, Food and Drug Administration, HFZ-133, 9200 Corporate Boulevard, Rockville, MD 20850.
E-mail: hsh@cdrh.fda.gov or hib@cdrh.fda.gov

Received November 21, 2000; Accepted June 15, 2001.

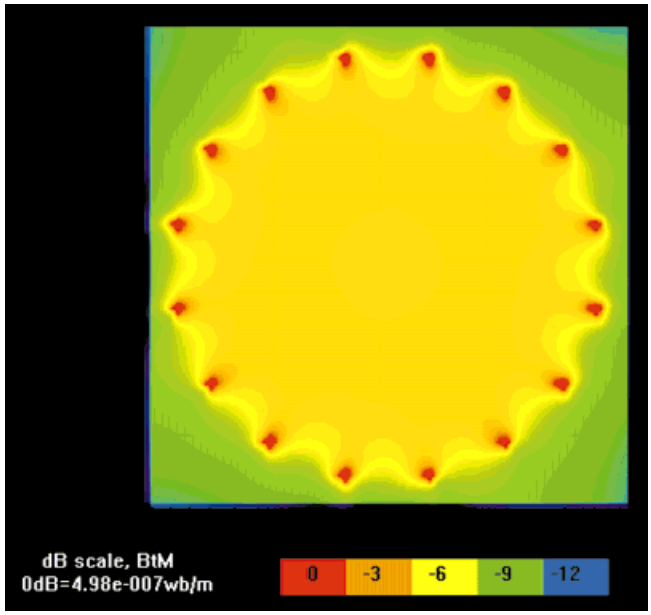

Figure 1. RF magnetic field (B_1) in the mid-transverse (x-y) plane of the birdcage coil. [Color figure can be viewed in the online issue, which is available at www.interscience.wiley.com.]

netic field problem in the time domain, using appropriate boundary conditions. SAR values in the human model were then computed from the induced electric field values. A Pentium II 450 MHz computer with 512 megabytes of memory was used for this calculation. The average time for each set of computations was approximately 2.5 days.

Theoretical Birdcage Coil

A theoretically represented MR birdcage body coil source was used for the computation of SAR distributions. The coil had a diameter of 70 cm and a length of 70 cm. It consisted of 16 wires, equally spaced, forming a circular cylinder, and terminated at each end of the wire cylinder with a circular wire (7). Hayes et al. (7) gave the details and a diagram of the original design of the birdcage body coil for the 1.5-Tesla MR imager.

The RF magnetic field of the coil source was induced by RF current sources at the midpoint of each of the 16 wires. The phase of the waveform of each current source shifted progressively with each wire around the wire cylinder, producing a uniform, circularly polarized RF magnetic field along the circular cross sectional plane inside the coil. The input impedance for each current source was 50 Ohms, in parallel with the current generator. The direction of the electric field inside the coil was along the length of the coil. The magnitude of the electric field inside the coil was highest near the surface of the coil and decreased toward the center of the coil.

The localized SAR values of this calculation were normalized to 1 W/kg whole body SAR value. This whole body SAR value was assumed to be determined experimentally, using a physical coil, taking into account the losses to the coil and to the environment. A physical coil would also require matching circuits to maximize the efficiency of the coil.

Realistic Human Model

The realistic human model was derived from the National Library of Medicine (NLM) Visible Human Project, which represents a large male with arms placed along his side, with his hands folded in front of his lap. The model is commercially available (5) in the form of a three-dimensional mesh of cells, suitable for the XFDTD calculation. The mesh is comprised of 136 × 98 × 319 cells. Each cell measures 5 mm × 5 mm × 5mm and represents a tissue type with appropriate dielectric properties. The dielectric property (8) of 23 types of tissues are used in the model.

RESULTS

The theoretically designed birdcage coil was tested for uniformity of the RF magnetic (B_1) field in the empty condition and by loading with an "imaging phantom". A uniform B_1 field was necessary to enable proper MR imaging performance of appropriate tissue models, including patients. Figure 1 shows the B_1 field in the empty birdcage coil produced by the array of 64 MHz current sources (1.5-Tesla MR scanner). Figure 2 shows the B_1 field in the birdcage coil loaded with an imaging phantom, which measured 30 cm × 30 cm × 5 cm and contained 0.6% aqueous NaCl solution with a conductivity of 1.3 S/m. The dimensions of the imaging phantom satisfied the minimum diameter requirement (20 cm) contained in the NEMA standard MS-3 (9). The results, as shown in Figure 1, indicate that the B_1 field was uniform in the empty birdcage coil to within ± 5%,

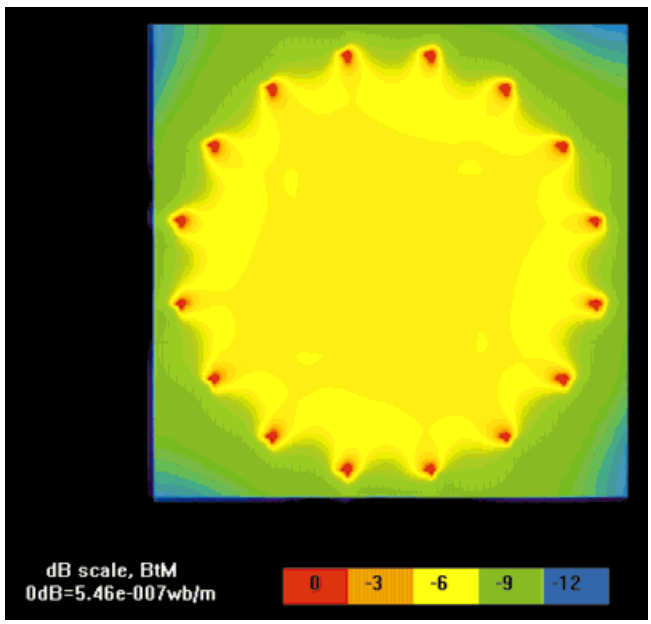

Figure 2. RF magnetic field in the mid-transverse (x-y) plane of the birdcage coil loaded with an imaging phantom. The RF magnetic field (B_1) was uniform to within ± 2.5% in the imaging phantom. [Color figure can be viewed in the online issue, which is available at www.interscience.wiley.com.]

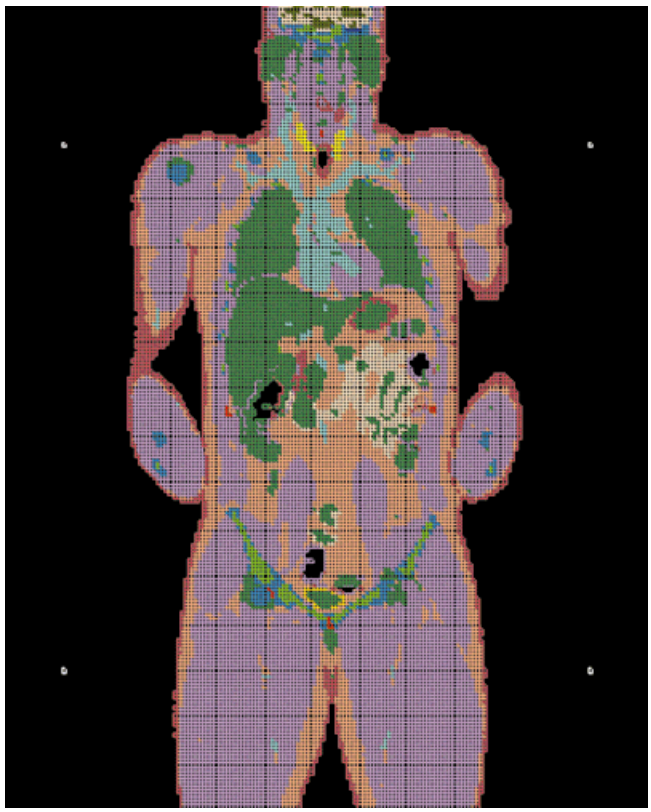

Figure 3. The mesh of the realistic human body along the mid-frontal plane (x-z) in the birdcage coil. The tissue types are color-coded. [Color figure can be viewed in the online issue, which is available at www.interscience.wiley.com.]

except in regions very close to the birdcage wires or near the ends of the coil. This uniformity should allow MR imaging in selected volumes interior to the birdcage coil. The B_1 field in the imaging phantom was found to be uniform to within ± 2.5%, which is also highly satisfactory for imaging.

Figure 3 shows the realistic human model along the mid-frontal (middle x-z) plane, with tissue types coded by color. Figure 4 shows the B_1 field along the mid-frontal (coronal) plane in the birdcage coil loaded with the realistic human model. The magnitude of the B_1 field is presented as color bands in 20% intervals. The B_1 field in the realistic human model, as shown, varied mostly within ± 10% (one color band).

The whole body averaged SAR value was set to 1 W/kg for all calculations. The SAR distributions along various cross-sections in the human model in a supine (face-up) position are shown in Figures 5 and 6. The SAR distribution in the mid-frontal (x-z) plane of the human model is shown in Figure 5. Most of the SAR heating occurred in muscle tissues near the periphery of the body, with a maximum SAR value of 16.5 W/kg for this plane. Some heating also occurred in tissues with high conductivity in the interior of the body. Figure 6 shows the SAR distribution along the transverse (x-y) plane near the waist region of the body. The SAR value of 31.6 W/kg was the maximum for the whole body and occurred as hot spots in muscle tissues near the waist, where the elbows touched the sides of the body.

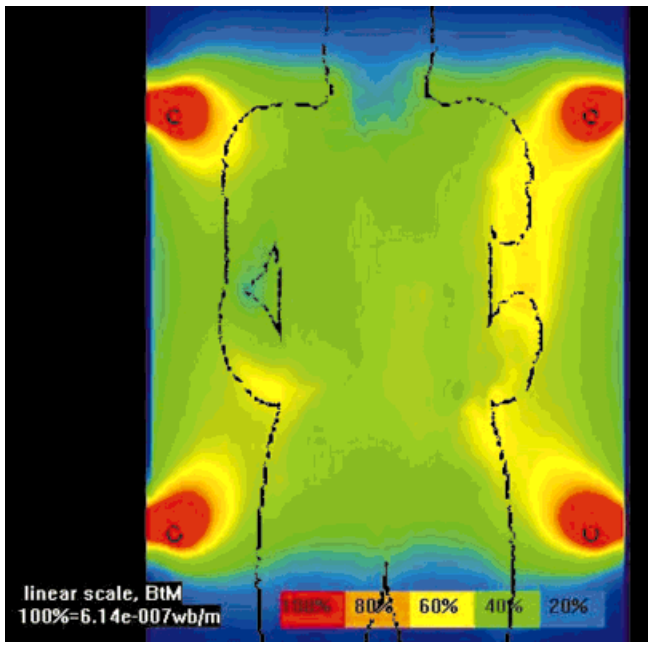

Figure 4. The RF magnetic field along the x-z plane in the middle of the birdcage coil loaded with the realistic human body model. Dark lines indicate the outline of the body cross section. [Color figure can be viewed in the online issue, which is available at www.interscience.wiley.com.]

The spatial peak SAR value of 31.6 W/kg was higher than the corresponding values of 12 W/kg in the extremities and 1.5 W/kg whole body averaged, under normal operating mode, contained in the IEC MRI

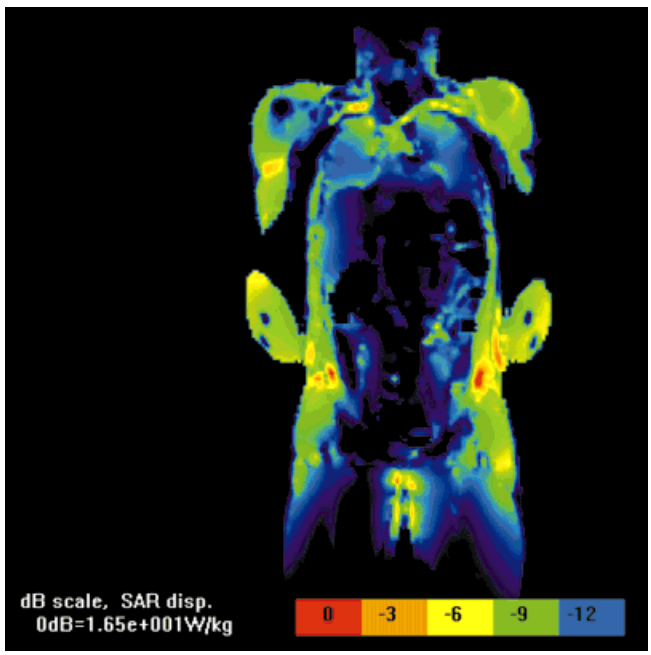

Figure 5. SAR distribution along the mid-frontal (x-z) plane of the realistic human model. The whole body averaged SAR value was 1 W/kg. The peak SAR value was 16.5 W/kg. [Color figure can be viewed in the online issue, which is available at www.interscience.wiley.com.]

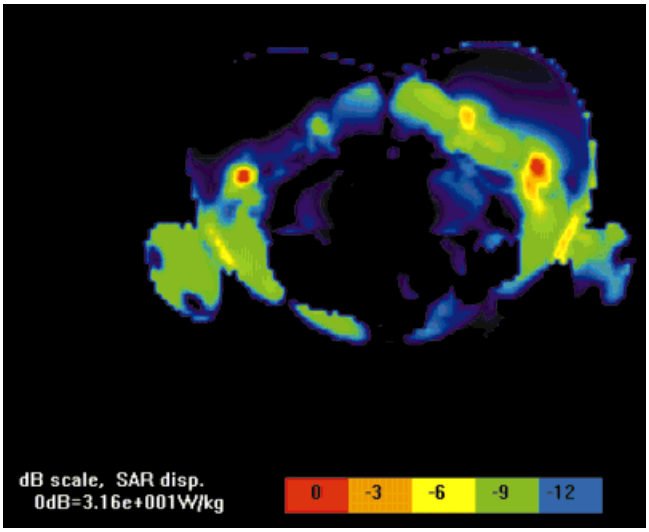

Figure 6. SAR distribution along the transverse (x-z) plane of the realistic human model near the waist region of the body. The whole body averaged SAR value was 1 W/kg. The peak SAR value for the whole body was 31.6 W/kg. [Color figure can be viewed in the online issue, which is available at www.interscience.wiley.com.]

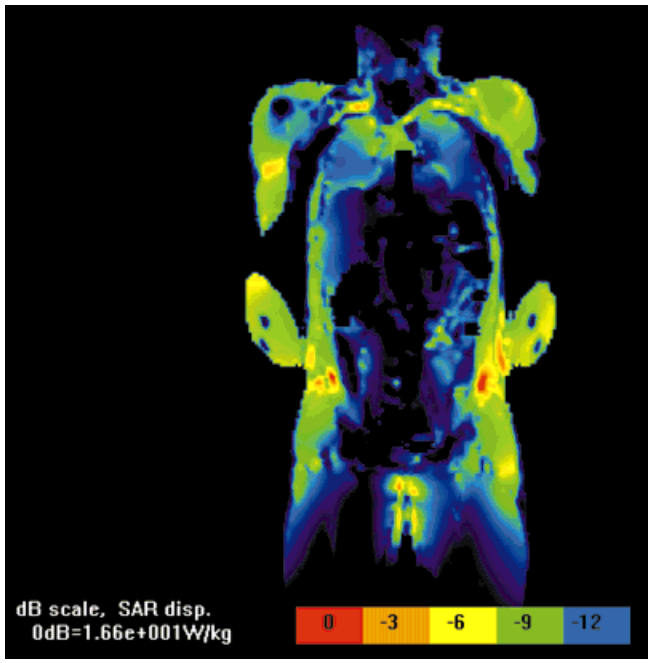

Figure 7. SAR pattern in the mid-frontal (middle x-z) plane of the realistic human model with a cylindrical metallic implant near the heart. The whole-body averaged SAR value was 1 W/kg. At locations near the implant, the maximum SAR value (at the upper tip of the implant) was 2.0 W/kg. [Color figure can be viewed in the online issue, which is available at www.interscience.wiley.com.]

safety standard (10). A smaller body and a different posture (hands not folded in front of the body) may result in different, perhaps lower, spatial peak SAR values. The XFDTD calculation did not consider the thermal diffusion properties of the human model. Therefore, the result of the calculation cannot be used directly to predict the potential local temperature rise in the patient. However, the result of the SAR calculation may be used to predict the locations with high SAR values in the body.

SAR Distributions in Realistic Human Model With Metallic Implants

Recently, there have been investigations of heating near implanted medical devices exposed to MR imaging (11,12). For the present calculation, a realistic human model was implanted with several metallic implants individually and then exposed to the RF magnetic field in the MR birdcage body coil. The SAR distributions in the human model were calculated to find possible enhanced RF heating in the surrounding tissues near the metallic implants.

Metallic Cylinder Implant

A metallic cylinder implant, 1 cm in diameter and 8 cm in length, was implanted in the heart region of the realistic human model. The resultant SAR distribution in the mid-frontal plane of the realistic human model is shown in Figure 7. The maximum SAR value near the metallic implant was 2.0 W/kg, compared to the value of 1.8 W/kg at the same location in the human model without the metallic implant. These data indicate that there was no appreciable increase of the RF heating in the surrounding tissues due to this metallic implant.

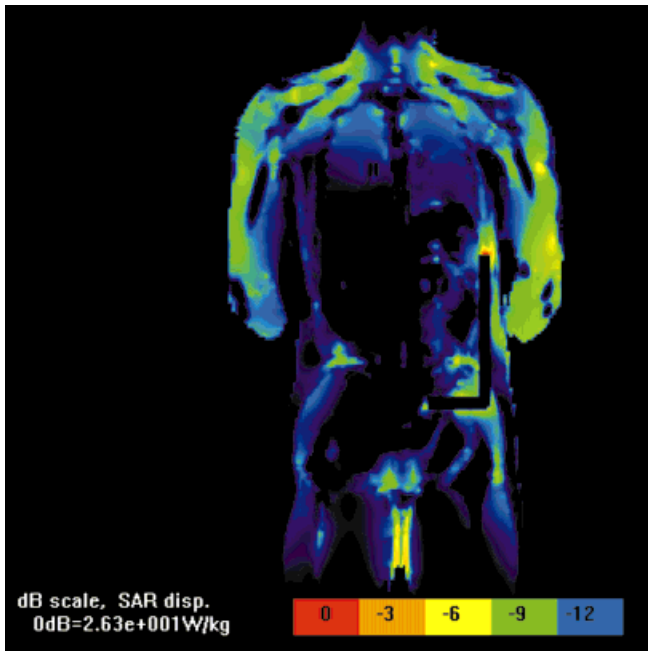

Figure 8. SAR pattern in the mid-frontal (middle x-z) plane of the realistic human model implanted with an L-shaped metallic thin wire near the base of the spinal column. The whole-body averaged SAR value was 1 W/kg. The maximum SAR value (at the upper tip of the implant) was 26.3 W/kg. [Color figure can be viewed in the online issue, which is available at www.interscience.wiley.com.]

Table 1
Maximum SAR Value Near the Tip of 1-cm Diameter Metallic Implant of Lengths 3, 6, 8, 12, and 24 cm in Regions of Low, Medium and High SAR Strength

Metallic implant length (cm)	SAR strength near implant	1-gram averaged SAR value near the tip of implant (W/kg)	1/8-gram averaged SAR value near the tip of implant (W/kg)
8	Low	2.0	2.0
24	Low	3.9	4.4
8	Medium	11.4	62
24	High	17.6	103
12	High	30.0	104
6	High	18.2	277
3	High	6.6	6.5

An additional calculation used a larger implant that was 24 cm long and 1 cm in diameter. No appreciable enhanced RF heating was produced with the implant near the heart region.

L-Shaped Metallic Thin Wire Implant

Another implant made of an L-shaped metallic thin 1-mm diameter wire was placed at the base of the spinal column of the realistic human model. The L-shaped wire was composed of a 9-cm horizontal section and a 24-cm vertical section. Figure 8 shows the SAR distribution in the frontal plane (x-z) bisecting the spinal column. The maximum SAR value near the tip of the vertical section of the implant was 26.3 W/kg compared to the value of 1.9 W/kg at the same location in the human model without the metallic implant. There was substantial enhanced RF heating due to the metallic implant in tissues surrounding the tip of the vertical section of the L-shaped wire. At the vertical tip of the L-shaped wire, the calculated single-point spatial-peak SAR value (averaged over 1/8 g of tissue) was 191 W/kg, which is significantly higher than the calculated averaged (over 1 g of tissue) SAR value of 26.3 W/kg.

Additional calculations, with only the horizontal section of the metallic wire implanted at the base of the spinal column of the human model, produce no appreciable enhanced RF heating.

Heating Due to Various Lengths of 1-cm and 1-mm Diameter Metallic Implants

The metallic implant, 1 cm or 1 mm in diameter, in various lengths of 3, 6, 8, 12, 24, and 34 cm were individually implanted in regions of low (the heart), medium (left side of the body), and high (right side of the body) SAR values. The maximum 1-g averaged and 1/8-g averaged SAR values are shown in Tables 1 and 2. The metallic cylinder implant in low SAR regions did not cause significant heating. However, in regions of medium and high SAR values, the metallic cylinder implant caused significant heating near the tip of the cylinder. This heating depended on the length of the cylinder; the 3-cm length implant did not cause significant heating.

DISCUSSION

The data from these calculations indicate that, in a MR imaging environment, enhanced RF heating of the patient occurs in tissues surrounding metallic implants. This finding agrees with the results of a recently published (13) experimental study of heating caused by pacemaker leads in a MR environment.

The calculation shows that the magnitude of the increased heating due to the presence of the metallic implant depends on the dimensions, orientation, shape, and location of the metallic implants in the patient.

For example, the vertical section of the L-shaped wire was parallel to the applied RF electric field of the birdcage coil. The external (applied) electric and magnetic fields produced by the birdcage coil induced the internal electric field in the patient. The wire was of sufficient length to cause coupling of the RF electric field in the patient to the wire and induced current flow in the wire, resulting in a high SAR value in surrounding tissues near the tip of the wire. The horizontal section of the wire did not seem to induce RF electric current flow

Table 2
Maximum SAR Value Near the Tip of 1-mm Diameter Metallic Implants of Lengths 3, 6, 12, 24 and 34 cm in Regions of Low, Medium and High SAR Strength

Metallic implant length (cm)	SAR strength near implant	1-gram averaged SAR value near the tip of implant (W/kg)	1/8-gram averaged SAR value near the tip of implant (W/kg)
24	Low	4.9	7.8
24	Medium	9.1	59
34	Medium	18.0	126
24	High	32.6	246
12	High	41.2	240
6	High	23.8	310
3	High	6.9	6.9

because it was oriented perpendicular to the applied RF electric field.

The metallic implant near the heart was parallel to the applied RF electric field of the birdcage coil. However, the implant was contained in a region of low SAR value, so that enhanced RF heating near the implant did not occur.

The SAR heating near the metallic implant primarily concentrated in a small volume at the tip of the metallic wire, resulting in a highly non-uniform enhanced RF heating of the surrounding tissues. For example, at the vertical tip of the L-shaped wire, the calculated single-point spatial-peak SAR value of 191 W/kg, averaged over 1/8 g of tissue, was significantly higher than the calculated spatial peak SAR value of 26.3 W/kg averaged over 1 g of tissue. The measurement of temperature rise near the tip of the implant may not reveal this high SAR value, which is concentrated in a relatively small volume (1/8 g) of tissue.

ACKNOWLEDGMENTS

The author thanks Howard Bassen and Loren Zaremba for the reviews and suggestions during the preparation of this manuscript.

REFERENCES

1. Magin RL, Liburdy RP, Persson B. Biological effects and safety aspects of nuclear magnetic resonance imaging and spectroscopy. Ann NY Acad Sci 1992;649:1–398.
2. Bottomley PA, Redington RW, Edelstein WA, Schenck JF. Estimating radiofrequency power deposition in body NMR imaging. Magn Reson Med 1985;2:336–349.
3. Chou CK, McDougall JA, Chan KW. RF heating of implanted spinal fusion stimulator during magnetic resonance imaging. IEEE Trans Biomed Eng 1997;44:367–372.
4. Shellock FG. MR-compatibility of an endoscope designed for use in interventional MRI procedures. AJR Am J Roentgenol 1998;171: 1297–1300.
5. Remcom, Inc. State College, PA. http://www.remcom.com/
6. Kunz KS, Luebbers RJ. The finite difference time domain method for electromagnetics. Boca Raton, FL: CRC Press; 1993. pp 1-448.
7. Hayes C, Edelstein WA, Schenck JF, Mueller OM, Eash M. An efficient, highly homogeneous radiofrequency coil for whole-body NMR imaging at 1.5 T. J Magn Reson Imaging 1985;63:622–628.
8. Armstrong Laboratory (AFMC), Brooks AFB, TX. http://www.brooks.af.mil/AFRL/HED/hedr/reports/dielectric/home.html
9. National Electrical Manufacturers Association. Determination of image uniformity in diagnostic magnetic resonance images, NEMA Standards Publication No. MS-3. Washington, DC: National Electrical Manufacturers Association; 1989. 12 p.
10. International Electrotechnical Commission. IEC 601-2-33 International standard part 2: particular requirements for the safety of magnetic resonance equipment for medical diagnosis. Geneva, Switzerland: International Electrotechnical Commission; 1998. 49 p.
11. Nyenhuis JA, Kildishev AV, Bourland JD, Foster KS, Graber GP, Athey TW. Heating near implanted medical devices by the MRI RF-magnetic field. IEEE Trans Magn 1999;35:4133–4135.
12. Smith CD, Kildishev AV, Nyenhuis JA, Foster KS, Bourland JD. Interactions of MRI magnetic fields with elongated medical implants. J Appl Physics 2000;87:6188–6190.
13. Sommer T, Vahlhaus C, Lauck G, et al. MR imaging and cardiac pacemakers: in vitro evaluation and in vivo studies in 51 patients at 0.5 T. Radiology 2000;215:869–879.